

## Systematic errors in waveform inversions caused by variable receiver coupling

Hansruedi Maurer\*, Stewart, A. Greenhalgh, Edgar Manukyan, Stefano Marelli, Alan, G. Green,  
Institute of Geophysics, ETH Zurich, Switzerland, maurer@aug.ig.erdw.ethz.ch

### Summary

The quality of receiver-to-ground coupling can be highly variable in surface, surface-to-borehole, and crosshole seismic experiments. Poor coupling can affect the recorded seismic traces in a major way. Ignoring variable coupling conditions can lead to severe problems when waveform inversions are attempted. To address such problems, we have developed a novel scheme that estimates medium properties and frequency-dependent source functions and frequency-dependent receiver-coupling factors. We demonstrate the efficacy of the new scheme via a synthetic crosshole experiment in which realistic receiver-coupling factors are simulated.

### Introduction

Seismic tomography is a powerful and versatile tool for a wide range of imaging applications in the earth sciences. Crosshole techniques are of particular interest for shallow and intermediate target depths. Typically, first-pulse traveltimes and amplitudes are inverted for subsurface velocity and attenuation properties.

Although waveform inversions were proposed more than 20 years ago (e.g., Tarantola, 1986; Mora, 1987), they only became popular quite recently (e.g., Plessix, 2008; Buske et al., 2009). The early algorithms were formulated in the time domain. Later, it was recognized that frequency domain inversion algorithms offer several advantages (e.g., Pratt, 1999; Zhou and Greenhalgh, 2003); with only a few frequencies, frequency-domain tomographic images comparable to their time-domain counterparts could be obtained at substantially lower computational costs. The success of frequency-domain inversions is primarily based on the fact that most seismic data are band limited, such that only a small number of frequencies are required for characterizing large parts of the entire waveforms.

The recent literature includes numerous synthetic studies, but it is noteworthy that only a few applications to real data have been reported. This is likely due to several systematic effects that require further research. For example, most waveform inversions are restricted to two dimensions, but the 3D radiation characteristics of most seismic sources requires at least a 2.5D problem to be solved (e.g., Zhou and Greenhalgh, 2006). Another well known problem concerns the generally unknown source characteristics. Several researchers have proposed algorithms that include

the unknown source function in the inversion process (e.g., Pratt, 1999; Ernst et al., 2007).

Whereas the need to invert for the generally unknown source function is well known, it is usually assumed that the response of the receivers can be ignored. This assumption may appear to be reasonable, because seismic receivers are typically selected to provide a flat response in the frequency band of interest. However, the receiver-to-ground coupling may influence the recordings significantly. More seriously, the coupling behavior may vary from sensor to sensor. This problem is highlighted in the two source gathers of Figure 1. The seismic traces in this figure were acquired in the framework of a time-lapse crosshole experiment designed for the non-intrusive monitoring of buried radioactive waste (Manukyan et al., 2008). Seismic energy was generated by a high-frequency sparker placed in a  $\sim 20^\circ$  downward-inclined borehole and the energy was received by a string of 24 hydrophones placed in a  $\sim 20^\circ$  upward-inclined borehole. Both boreholes were water filled. More details on this experiment can be found in Marelli et al. (2010). During the acquisition of the first suite of data (example traces are shown in blue in Figure 1), the location of the hydrophone string was fixed and the sparker was sequentially ignited at 24 positions along the source borehole. Immediately afterwards, the hydrophone string was removed and reinserted at the same position in the receiver borehole (to within  $< 3$  cm). The second suite of measurements (example traces are shown in red in Figure 1) were made by igniting the sparker at the same source positions (to within  $< 3$  cm). The elastic parameters within the area of interest did not change between the two experiments, and extensive tests demonstrated that the repeatability of the seismic source was very good (Marelli et al. 2010). Consequently, variable receiver coupling must have produced the very significant differences between the blue and red traces. The astonishingly large differences are likely caused by minor changes in the seating of the hydrophones on the borehole wall; note, that we have also observed similar (although smaller) effects in data received by hydrophones hanging freely in vertically oriented boreholes.

The variable receiver coupling does not create problems for traveltimes inversions (the first breaks of the two suites of traces are identical to within less than 0.05 ms), but the differences in the later parts of the waveforms will substantially affect waveform inversions. As a result of our experiments, we consider that it is necessary to have a waveform inversion algorithm that is capable of simultaneously estimating medium properties and

## Receiver coupling and waveform inversions

frequency-dependent source functions and frequency-dependent receiver-coupling factors. We present such an algorithm and demonstrate its performance on a realistic synthetic data set.

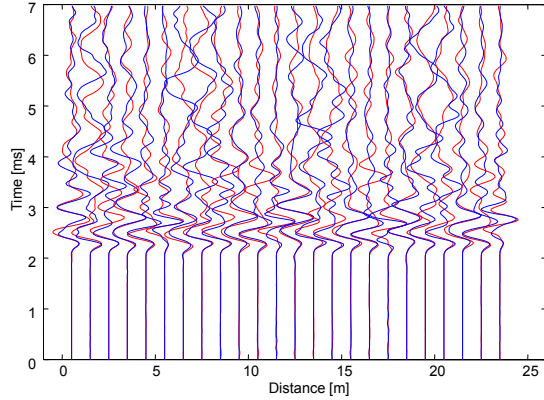


Figure 1: Results from a reinsertion experiment using a sparker source and a hydrophone string. The blue traces show a source gather from the first experiment and the red traces show the repeat source gather after reinserting the hydrophone streamer. Distance of the source from the borehole mouth is shown on the horizontal axis. Average source-receiver distances are 10-15 m. Note, that the first breaks were horizontally aligned for display purposes.

### Simultaneous estimation of medium properties, source functions, and receiver-coupling factors

For the sake of simplicity, we consider a 2D acoustic and constant-density problem that will be analyzed in the frequency domain. The observed and predicted data  $d^{obs,pred}$  can be thus written as the product

$$(1) \quad d_{ij}(\omega) = s_i(\omega) \cdot G_{ij}(\mathbf{m}, \omega) \cdot r_j(\omega),$$

where  $i$  and  $j$  are the source and receiver indices,  $\omega$  is frequency,  $s_i$  and  $r_j$  represent the unknown source functions and receiver-coupling factors respectively,  $G_{ij}$  are the Green's functions that characterize wave propagation between the  $i$ th source and the  $j$ th receiver, and the vector  $\mathbf{m}$  contains the medium properties (i.e., P-wave velocities).

To invert for the medium properties alone, an iterative Gauss-Newton type algorithm can be employed (e.g., Pratt et al., 1998)

$$(2) \quad \mathbf{m}_{k+1}^{est} = (\mathbf{J}^T \mathbf{J} + \mathbf{C}_M^{-1})^{-1} \mathbf{J}^T \left[ (\mathbf{d}^{obs} - \mathbf{d}^{pred}) + \mathbf{J} \mathbf{m}_k^{est} \right],$$

where the superscript *est* indicates estimated (inverted) quantities.  $\mathbf{J}$  is the Jacobian matrix that includes the partial derivatives of the data with respect to the model parameters for the  $k$ th iteration, and  $\mathbf{C}_M^{-1}$  is the a priori model covariance matrix that includes the regularization constraints. A possible strategy to account for the unknown source functions and receiver-coupling factors would be to include them in the inversion as additional model parameters. This would require the vector  $\mathbf{m}$  to be augmented with  $ns \times n\omega$  source functions and  $nr \times n\omega$  receiver-coupling factors, where  $ns$ ,  $nr$  and  $n\omega$  indicate the number of sources, receivers, and frequencies respectively. The partial derivatives with which the Jacobian matrix would have to be augmented would be:

$$(3) \quad \frac{\partial d_{ij}}{\partial s_i} = G_{ij} \cdot r_j \quad \text{and} \quad \frac{\partial d_{ij}}{\partial r_j} = G_{ij} \cdot s_i.$$

Because of pronounced non-linearities in the waveform inversion problem, such an approach proved to be unstable. Furthermore, the size of the Hessian matrix  $\mathbf{J}^T \mathbf{J}$  would be increased significantly if several frequencies and a large number of sources and receivers were to be included.

To resolve this issue, we have designed a robust source-function and receiver-coupling estimation scheme that can be applied prior to the Gauss-Newton inversion step in equation (2). Initially, the receiver-coupling factors  $\mathbf{r}$  are set to 1.0 and a first estimate of the Green's function  $G_{ij}$  is calculated, for example, using a model  $\mathbf{m}^{ini}$  based on travelttime inversion of the first breaks. A first estimate of  $\mathbf{s}$  is then made using:

$$(4) \quad s_i^{est}(\omega) = \text{mean} \left( \frac{d_{ij}^{obs}(\omega)}{G_{ij}(\omega) \cdot r_j^{ini}(\omega)} \right).$$

Subsequently,  $s_i^{ini}$  is set equal to  $s_i^{est}$  and first estimates of the receiver-coupling factors are made using:

$$(5) \quad r_j^{est}(\omega) = \text{mean} \left( \frac{d_{ij}^{obs}(\omega)}{G_{ij}(\omega) \cdot s_i^{ini}(\omega)} \right).$$

Values of  $r_j^{est}$  are assigned to  $r_j^{ini}$  and the procedure is repeated until convergence is achieved (typically after 3 - 5 iterations). The predicted data  $\mathbf{d}^{pred}$  computed from equation 1 using  $\mathbf{m}^{ini}$  and the "final" estimated source functions and receiver-coupling factors are then the basis for the Gauss-Newton inversion in equation 2. The procedure described above (equations 4 and 5) needs to be repeated prior to every inversion step  $k$  (equation 2).

## Receiver coupling and waveform inversions

The computation of the mean values in equations 4 and 5 is equivalent to a least-squares (L2 norm) inversion for the parameters  $s_i^{est}$  and  $r_j^{est}$ . One could obtain a more robust L1 norm estimate (e.g., Rice and White, 1964) by simply replacing the *mean()* by the *median()* operator in equations 4 and 5.

### A synthetic example

The experimental configuration for the simulations is shown in Figure 2. It includes 26 sources and 26 receivers distributed along two boreholes within a medium that contains positive and negative cross-shaped velocity anomalies. The source is a Ricker wavelet with a central frequency of 1500 Hz. Figure 3a shows the resulting seismic traces for the shot position at 18 m depth. The blue traces represent the simulations using the heterogeneous model in Figure 2, whereas the black traces would be obtained for a homogeneous 2000 m/s model. In Figure 3b, the blue traces are repeated from Figure 2 and red traces are the same as the blue ones except that realistic receiver-coupling factors have been added. The statistics of these factors mimic those of the observed variations in Figure 1. Clearly, the receiver-coupling variations overwhelm the effects of the velocity anomalies (i.e., the differences between the red and blue traces are larger than those between the blue and black traces).

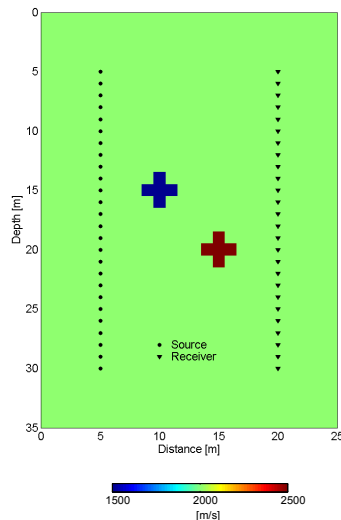


Figure 2: Velocity model and source-receiver configuration employed for the synthetic example.

For the inversion of the synthetic data, we started with three low frequencies (200, 300, and 400 Hz) and then

progressively added frequencies up to 2000 Hz. For the final iteration steps only 8 frequencies were employed.

Velocity tomograms based on 3 waveform-inversion scenarios are presented in Figure 4. For Figure 4a, the known synthetic source function and receiver-coupling factors are employed in equation 1 (i.e., equations 4 and 5 are not required). The two crosses are well resolved in this tomogram. For Figure 4b, the known synthetic receiver-coupling factors are used in equation 1 (i.e., equation 5 is not required), but the "unknown" source function is determined from iterative solutions of equation 4. Although there are minor artifacts along the source and receiver boreholes, the two crosses are again well resolved. Finally, P-wave velocities and "unknown" source functions and "unknown" receiver-coupling factors are determined during the computation of the tomogram in Figure 4c, the quality of which is comparable to that in Figure 4b.

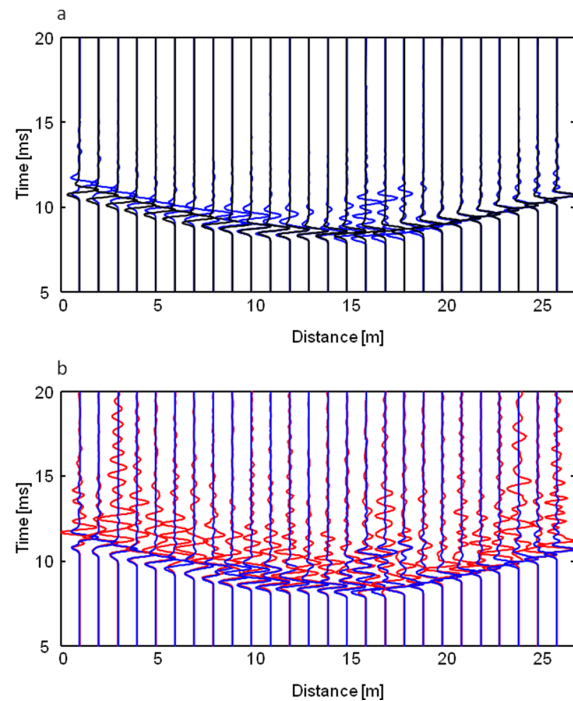


Figure 3: a) Black traces are source gather for the shot position at 18 m depth and a homogeneous velocity model (2000 m/s), whereas the blue traces are a source gather for the same shot position and the heterogeneous model in Figure 2. b) The blue traces are the same as in a) and the red ones are for the velocity model in Figure 2 with realistic receiver-coupling factors.

Waveform inversion of the synthetic data without prior knowledge of the receiver coupling factors and without

## Receiver coupling and waveform inversions

taking account of them fails to produce a meaningful tomogram (not shown).

The tomograms in Figure 4 are based on inversions using 8 frequencies. With knowledge of the recovered velocity structure (i.e., knowledge of the Green's functions  $G_{ij}$ ), the source functions and receiver-coupling factors can be estimated for a full-range of frequencies using equations 4 and 5. This allows us to compute predicted traces via equation 1 and an inverse Fourier transform. Figure 5 demonstrates the excellent fit of the resultant predicted traces (blue) with the original traces (red) for the shot at 18 m depth.

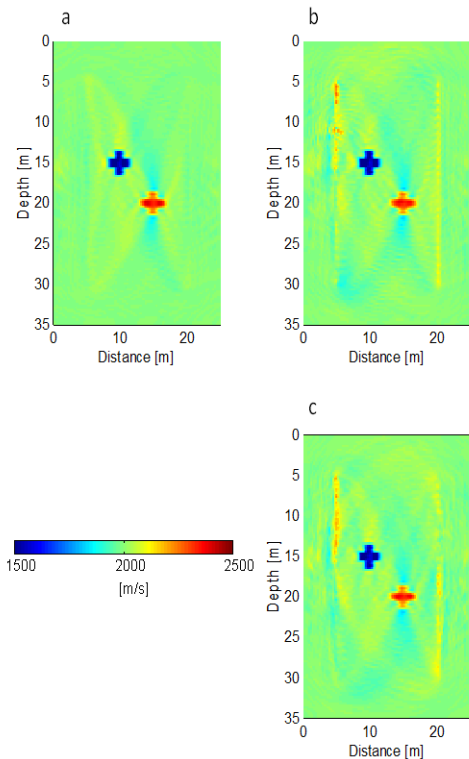


Figure 4: Tomographic inversion results. Tomograms obtained with a) known source functions and known receiver-coupling factors, b) unknown source functions and known receiver-coupling factors, and c) unknown source functions and unknown receiver-coupling factors.

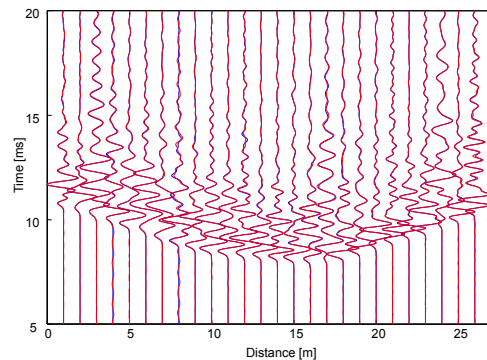


Figure 5: Comparison of original traces (red; same as in Figure 3b) and predicted traces using the tomogram in Figure 4c and the associated source functions and receiver-coupling factors.

## Conclusions

A variety of field experiments have indicated that receiver-coupling effects can be very significant, probably distorting waveform inversions in a major way. Our scheme for estimating unknown source functions and receiver-coupling factors provides a powerful tool for addressing this problem. The scheme has been applied to 2D synthetic acoustic data, but conceptually the methodology can be extended in a relatively straightforward fashion to 2.5D and 3D elastic, visco-elastic, and anisotropic media; the scheme for estimating the source function and receiver-coupling factors is only weakly linked to the tomographic inversion algorithm.

Computation of the source functions and receiver-coupling factors using equations 4 and 5 is computationally very efficient, requiring an insignificant amount of computing time compared to that required to calculate the predicted waveforms, the sensitivities, and the Gauss-Newton inversion steps. Consequently, such an estimation scheme (or variant thereof) could be included in every waveform inversion procedure.

## Acknowledgments

This work was carried out in the framework of the EC projects ESDRED and ModDeRn. We acknowledge the financial support of the European Commission, NDA, NAGRA and ETH.

## EDITED REFERENCES

Note: This reference list is a copy-edited version of the reference list submitted by the author. Reference lists for the 2010 SEG Technical Program Expanded Abstracts have been copy edited so that references provided with the online metadata for each paper will achieve a high degree of linking to cited sources that appear on the Web.

## REFERENCES

- Buske, S., I. Lecomte, T. Nemeth, S. Operto, and V. Sallares, 2009, Imaging and inversion – Introduction: *Geophysics*, **74**, no. 6, WCA1–WCA4, [doi:10.1190/1.3256872](https://doi.org/10.1190/1.3256872).
- Ernst, J. R., A. G. Green, H. Maurer, and K. Holliger, 2007, Application of a new 2D time-domain full-waveform inversion scheme to crosshole radar data: *Geophysics*, **72**, no. 5, J53–J64, [doi:10.1190/1.2761848](https://doi.org/10.1190/1.2761848)
- Manukyan, E., H. R. Maurer, S. Marelli, S. A. Greenhalgh, and A. G. Green, Non-intrusive monitoring using seismic tomography at the Mont Terri rock laboratory: Annual meeting, SEG.
- Marelli, S., E. Manukyan, H. R. Maurer, S. A. Greenhalgh, and A. G. Green, 2010, Appraisal of waveform repeatability and reliability for crosshole and hole-to-tunnel seismic monitoring of radioactive waste repositories: *Geophysics*, (subject to revision.).
- Mora, P., 1987, Nonlinear Two-Dimensional Elastic Inversion of Multioffset Seismic Data: *Geophysics*, **52**, 1211–1228, [doi:10.1190/1.1442384](https://doi.org/10.1190/1.1442384).
- Plessix, R.-E., 2008, Introduction: Towards a full waveform inversion: *Geophysical Prospecting*, **56**, no. 6, 761–763, [doi:10.1111/j.1365-2478.2008.00736.x](https://doi.org/10.1111/j.1365-2478.2008.00736.x).
- Pratt, R. G., 1999, Seismic waveform inversion in the frequency domain, Part 1: Theory and verification in a physical scale model: *Geophysics*, **64**, 888–901, [doi:10.1190/1.1444597](https://doi.org/10.1190/1.1444597).
- Pratt, R. G., C. Shin, and G. J. Hicks, 1998, Gauss-Newton and full Newton methods in frequency-space seismic waveform inversion: *Geophysical Journal International*, **133**, no. 2, 341–362, [doi:10.1046/j.1365-246X.1998.00498.x](https://doi.org/10.1046/j.1365-246X.1998.00498.x).
- Rice, J. R., and J. S. White, 1964, Norms for Smoothing + Estimation: *SIAM Review*, **6**, no. 3, 243, [doi:10.1137/1006061](https://doi.org/10.1137/1006061).
- Tarantola, A., 1986, A Strategy for Nonlinear Elastic Inversion of Seismic-Reflection Data: *Geophysics*, **51**, 1893–1903, [doi:10.1190/1.1442046](https://doi.org/10.1190/1.1442046).
- Zhou, B., and S. Greenhalgh, 2006, An adaptive wavenumber sampling strategy for 2.5D seismic-wave modeling in the frequency domain: *Pure and Applied Geophysics*, **163**, no. 7, 1399–1416, [doi:10.1007/s00024-006-0081-7](https://doi.org/10.1007/s00024-006-0081-7).
- Zhou, B., and S. A. Greenhalgh, 2003, Crosshole seismic inversion with normalized full-waveform amplitude data: *Geophysics*, **68**, 1320–1330, [doi:10.1190/1.1598125](https://doi.org/10.1190/1.1598125).